Appl Phys B (2010) 98: 165–172
DOI 10.1007/s00340-009-3766-7

Applied Physics B
Lasers and Optics

Infrared luminescence, thermoluminescence and defect centres in Er and Yb co-doped $ZnAl_2O_4$ phosphor

V. Singh · S. Watanabe · T.K. Gundu Rao · J.F.D. Chubaci · I. Ledoux-Rak · H.-Y. Kwak

Received: 24 April 2009 / Published online: 8 October 2009

Abstract Er and Yb co-doped $ZnAl_2O_4$ phosphors were prepared by solution combustion synthesis and the identification of Er and Yb were done by energy-dispersive X-ray analysis (EDX) studies. A luminescence at 1.5 μm, due to the $^4I_{13/2} \rightarrow {}^4I_{15/2}$ transition, has been studied in the NIR region in Er and Yb co-doped $ZnAl_2O_4$ phosphors upon 980 nm CW pumping. Er-doped $ZnAl_2O_4$ exhibits two thermally stimulated luminescence (TSL) peaks around 174°C and 483°C, while Yb co-doped $ZnAl_2O_4$ exhibits TSL peaks around 170°C and 423°C. Electron spin resonance (ESR) studies were carried out to identify defect centres responsible for TSL peaks observed in the phosphors. Room temperature ESR spectrum appears to be a superposition of two distinct centres. These centres are assigned to an O^- ion and F^+ centre. O^- ion appears to correlate with the 174°C TSL peak and F^+ centre appears to relate with the high temperature TSL peak at 483°C in $ZnAl_2O_4$:Er phosphor.

PACS 78.55.-m · 32.50.+d · 42.62.-b · 81.20.Ka

V. Singh (✉) · I. Ledoux-Rak
Laboratoire de Photonique Quantique et Moleculaire, UMR CNRS 8537, Institut d'Alembert, Ecole Normale Superieure de Cachan, 61 av. du President-Wilson, 94235, Cachan, France
e-mail: vijayjiin2006@yahoo.com

V. Singh · H.-Y. Kwak (✉)
Mechanical Engineering Department, Chung-Ang University, Seoul 156-756, South Korea
e-mail: kwakh@cau.ac.kr

S. Watanabe · T.K. Gundu Rao · J.F.D. Chubaci
Institute of Physics, University of Sao Paulo, 05508-090, Sao Paulo, SP, Brazil

1 Introduction

Zinc aluminate spinel ($ZnAl_2O_4$) is a well-known wide-band gap semiconductor ($E_g = 3.8$ eV) material having high thermal stability, high mechanical resistance, low surface acidity and due to these properties it has been widely used as opto-mechanical, catalyst, ceramic, anti-thermal coating in aero-space vehicles and electro-conductive materials [1–5]. Zinc aluminate spinel also has UV opto-electronic applications [6, 7].

It is well known that rare-earth doped inorganic materials exhibit a variety of point defects stabilised due to the charge imbalance/self-irradiation and they play an important role in luminescence properties [8–10]. In recent years several types of localised excitons are identified and their decay into electron and hole centres are found [11–14]. The trapping centres or defect properties of a potential laser material and for the after glow of inorganic phosphors are very important, since the optical performance is usually significantly influenced by the defect centres. The origin of the centres, created at the decay of the self-trapped and localised exciton states and the defect-related states, is studied by using the techniques of electron spin resonance (ESR) and thermally stimulated luminescence (TSL) [15–18]. The defects created by ionising radiation are studied by several researchers [19–23]. Recently we have reported the TSL and ESR studies on the rare-earth doped inorganic phosphors, wherein the nature of the defects formed on irradiation in these phosphors and their role in the thermally stimulated relaxation processes leading to TSL are presented [24–26].

Recently, the near-infrared (NIR) luminescence from lanthanide-doped materials are gaining increasing interest due to their potential applications. Among lanthanides, NIR luminescence from Er^{3+} ions proves very useful when employed in telecommunication network optical signal ampli-

fiers [27–29]. In general, luminescence from Er-doped semiconductors suffers from its low emission intensity at room temperature and thus their application to light-emitting devices seems to be difficult. It is well known that Yb^{3+} acts as a sensitiser of Er^{3+} emission and several papers regarding Er and Yb co-doped phosphors have been published [30–34]. In the present investigation we have also used Yb as a co-dopant. Due to the wide-band gap and spinel structure of $ZnAl_2O_4$, it is possible to incorporate a large variety of rare-earth and transition metal ions as dopants. There is no report on the visible and near-infrared luminescence of Er and Yb co-doped $ZnAl_2O_4$ phosphor as far as we know. Also there is no report on the identification of the radiation-induced radicals/defect centres formed on irradiation and the subsequent electron–hole recombination reactions resulting in the glow peaks on this sample. In the present study, we have carried out TSL and ESR investigations on gamma irradiated Er and Yb co-doped $ZnAl_2O_4$ phosphors. The nature of the defects formed on gamma irradiation in these phosphors and their role in thermally stimulated relaxation processes have been investigated. Luminescence studies have shown that the Er^{3+} and Yb^{3+} centres act as a luminescent centres.

2 Experimental details

Two phosphors according to the chemical formula $ZnAl_2O_4$:Er (0.02 mol%) and $ZnAl_2O_4$:Er, Yb (0.02, 0.05 mol%) were prepared by using the solution combustion method. Stoichiometric amounts of nitrates of zinc, aluminium, erbium and ytterbium were thoroughly mixed with urea. The nitrate to urea ratios were determined on the basis of total oxidising (O) and reduction (F) valencies of the components so that the equivalence ratio $\emptyset e$ is unity (i.e. $O/F = 1$) and the energy released by the combustion is at a maximum [35]. The starting materials were mixed in a minimum volume of deionised water in a pyrex dish of approximately 200 ml capacity and the solution was rapidly heated in a muffle furnace which was preheated to 500°C. Within minutes the solution foamed and a flame was produced which lasted for several seconds. The pyrex dish was immediately removed from the furnace. The resultant fluffy mass was ground crushed into powder and the resulting fine powder was used for characterisation. The formation of Er and Yb co-doped $ZnAl_2O_4$ phosphors was confirmed by comparing the X-ray diffraction (XRD) diffractograms with the standard data (JCPDS file No. 82-1043).

The powders were taken in an adhesive tape fixed onto a stub for electron microscopic evaluation. As they are non-conductive, the powders were coated with graphite and chemical compositions were analysed using the EDX attached to the SEM (S-3400, Hitachi, Japan).

The IR photoluminescence emission spectrum was studied using a Jobin-Yvon HR 460 monochromator with a 900 grooves/mm grating coupled to a Triax 320 multichannel CCD detection set-up for infrared measurements. Samples were pumped using a CW diode laser from BW TEK operating at 980 nm and delivering a power ranging from 0 to 1 W. All optical measurements were performed at room temperature.

A ^{60}Co gamma source was used for the irradiation of samples. TSL experiments were carried out on a Daybreak 1100 series automated TSL reader system with a heating rate of 5°C/s in a nitrogen atmosphere. A Bruker EMX ESR spectrometer operating at X-band frequency with 100 kHz modulation frequency was utilised for ESR experiments. Diphenyl Picryl Hydrazyl (DPPH) was used for calibrating the g-values of the defect centres. Temperature dependence of the ESR spectra was studied using a Bruker B VT 2000 variable temperature accessory.

3 Results and discussion

3.1 EDX study

To confirm the presence of Er and Yb in $ZnAl_2O_4$, energy-dispersive X-ray (EDX) analyses were conducted on these phosphors and are shown in Figs. 1 and 2. The samples were imaged using Back Scattered Electron detection mode and entire area of the micrographs (BSE) was analysed for EDX mapping and spectrum. The peaks in the spectra reveal the presence of Er, Zn, Al, O in Er-doped $ZnAl_2O_4$ (Fig. 1a) and Er, Yb, Zn, Al, O in Yb co-doped $ZnAl_2O_4$:Er (Fig. 1b), respectively. The chemical composition ratio derived from the EDX spectra was found to be very close to the nominal composition values $ZnAl_2O_4$:$Er_{0.02}$ and $ZnAl_2O_4$:$Er_{0.02}Yb_{0.05}$. EDX mapping of as-prepared Er and Yb co-doped $ZnAl_2O_4$ powders are presented in Fig. 2. Figure 2a shows the elemental mapping of Er, Zn, Al, O for Er-doped $ZnAl_2O_4$ and the mapping of Er, Yb, Zn, Al, O for Yb co-doped $ZnAl_2O_4$:Er is shown in Fig. 2b. These mappings show homogeneous distribution of each element in the phosphors. Further, in order to know the distribution of Er in $ZnAl_2O_4$:Er and Er and Yb in $ZnAl_2O_4$:Er, Yb the overlapping of BSE and EDX mapping for Er and Er, Yb are shown in Fig. 2b, BSE + Er and Fig. 2b, BSE + Er + Yb, respectively. It is clear from these micrographs that the dopant ions are well dispersed. This result of EDX shows that low temperature combustion method is quite effective in order to incorporate Er and Yb in $ZnAl_2O_4$ host, even with low doping concentration. Recently, it has been reported that a homogeneous Er^{3+} ion distribution in a host matrix is essential in order to achieve an efficient amplification [36]. In the present phosphors, it is observed that the dopants are well dispersed in the $ZnAl_2O_4$ matrix.

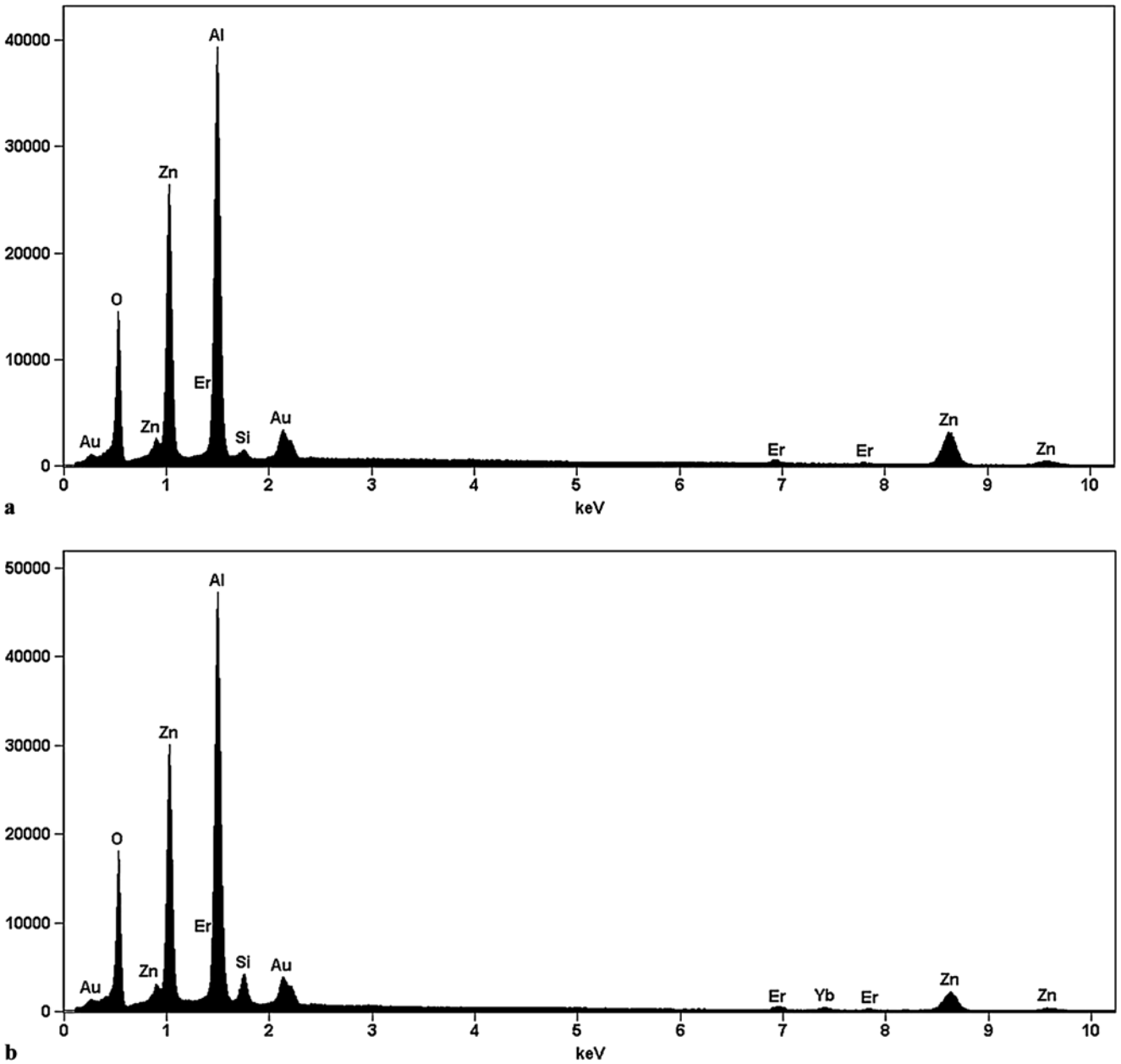

Fig. 1 EDX spectrum of as-synthesised (**a**) $ZnAl_2O_4$:Er and (**b**) $ZnAl_2O_4$:Er, Yb phosphor

3.2 NIR luminescence of $ZnAl_2O_4:Er^{3+}$ phosphor co-doped with Yb^{3+}

Figure 3 shows the photoluminescence spectra in the infrared region of Er and Yb co-doped $ZnAl_2O_4$ phosphors at room temperature. The broad band extending from 1.45 to 1.65 μm and centred at 1.5 μm is attributed to $^4I_{13/2} \rightarrow {}^4I_{15/2}$ transition of Er^{3+} ion upon 980 nm CW excitation at different pump power values. It is observed that the addition of Yb^{3+} in $ZnAl_2O_4$:Er phosphor enhances the intensity of the emission band by more than 10 times (Fig 3b). The reason for the use of co-doped $ZnAl_2O_4$ phosphors is essentially to take advantage of the fact that Yb^{3+} acts as a sensitiser for Er^{3+}. Further, high concentration of Er^{3+} ions is required for sufficient amplification, but Er^{3+} ions tend to cluster even at moderate concentrations. To circumvent this problem, co-doping with Yb^{3+} ions is normally used. In addition the $^2F_{7/2} \rightarrow {}^2F_{5/2}$ transition of Yb^{3+} exhibits a strong cross section around 0.98 μm, which enhances considerably the pumping efficiency. The $^2F_{7/2}$ level of Yb^{3+} is in close proximity to the $^4I_{11/2}$ level of Er^{3+} promoting an efficient energy transfer between Yb^{3+} and Er^{3+}. The use of Yb^{3+} and Er^{3+} co-doped systems takes advantage of the existence of a suitable absorption band for the pumping

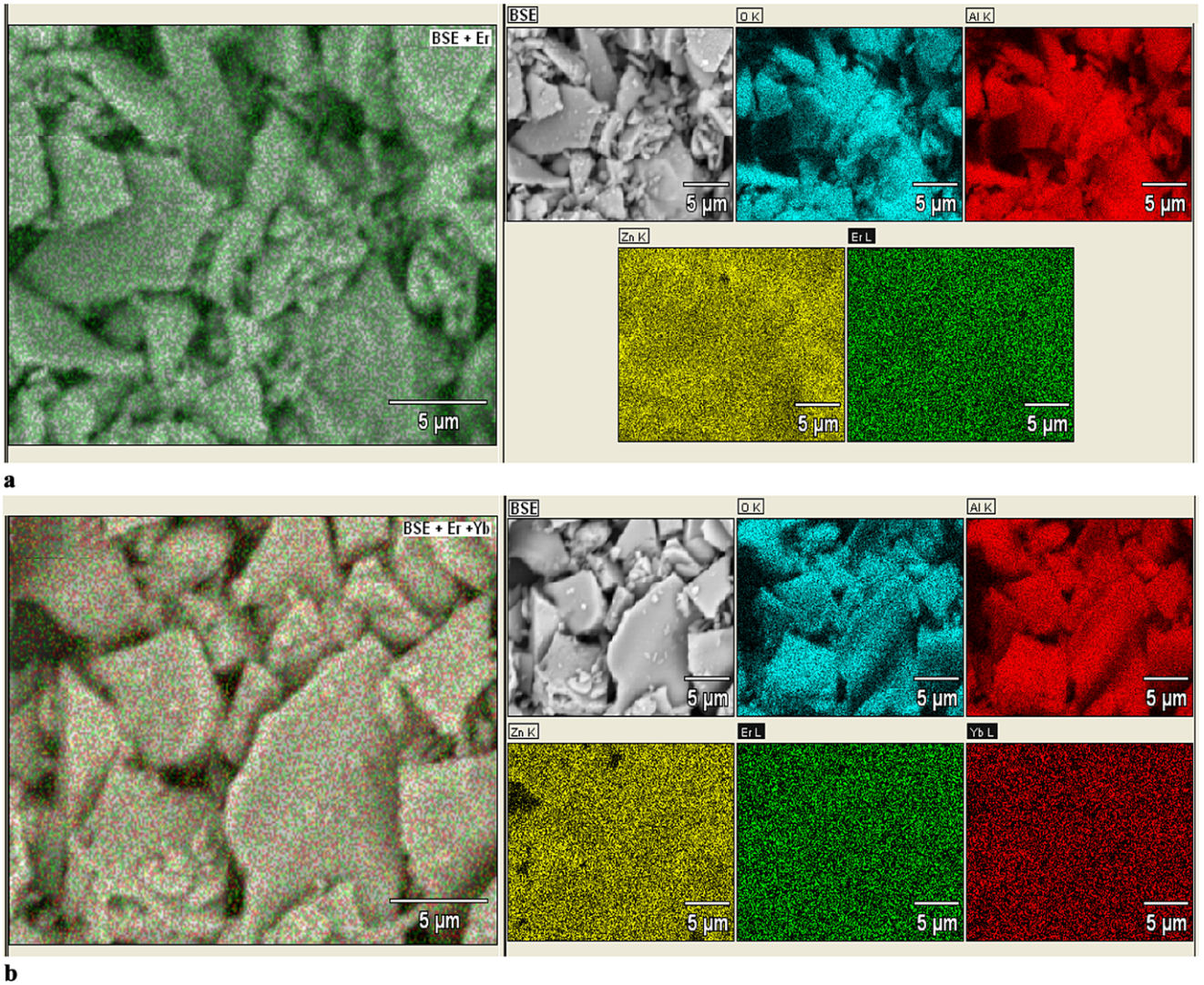

Fig. 2 EDX mapping of (**a**) $ZnAl_2O_4$:Er and (**b**) $ZnAl_2O_4$:Er, Yb phosphor

source as well as an efficient $Yb^{3+} \rightarrow Er^{3+}$ energy transfer, a mechanism which is known for a long time. We have also examined the intensity variation of 1.5 µm emission as a function of the laser intensity. The emission intensity as a function of laser intensity shows a linear behaviour in the investigated range. It should be noted that the full width at half maximum (FWHM) of the $^4I_{13/2} \rightarrow {}^4I_{15/2}$ transition for the Er and Yb co-doped $ZnAl_2O_4$ phosphors is about 67 nm. Such a broad emission band is desirable for optical amplification [37]. It is seen from the present results that co-doping enhances significantly the luminescence intensity.

3.3 TSL and ESR of $ZnAl_2O_4:Er^{3+}$ phosphor co-doped with Yb^{3+}

Prior to gamma irradiation no glow peaks were observed in Er and Yb co-doped $ZnAl_2O_4$ phosphors. However, upon gamma irradiation to a dose of 100 Gy, $ZnAl_2O_4:Er^{3+}$ exhibits TSL peaks around 174°C and 483°C (Fig. 4a) while Yb co-doped $ZnAl_2O_4$:Er exhibits TSL peaks around 170°C and 423°C (Fig. 4b). The glow curves for the samples were obtained at a heating rate of 5°C/s. High temperature peaks were found to be more intense in both the phosphors. It is to be noted that the addition of Yb^{3+} in $ZnAl_2O_4$:Er phosphor enhances the intensity of TSL peaks and also it is observed that the TSL peaks are shifting towards low temperatures. It has been possible to achieve an efficient resonant energy transfer with Yb^{3+} co-doping in $ZnAl_2O_4$ phosphor.

Figure 5a shows the ESR spectrum at room temperature after gamma irradiation (dose: 5000 Gy) of $ZnAl_2O_4$:Er phosphor. The observed spectrum appears to be superposition of at least two distinct centres. This inference is based on thermal annealing experiments. It was possible to identify two centres and these are labelled in Fig. 5a. The ESR line labelled as Centre I is due to a centre characterised by

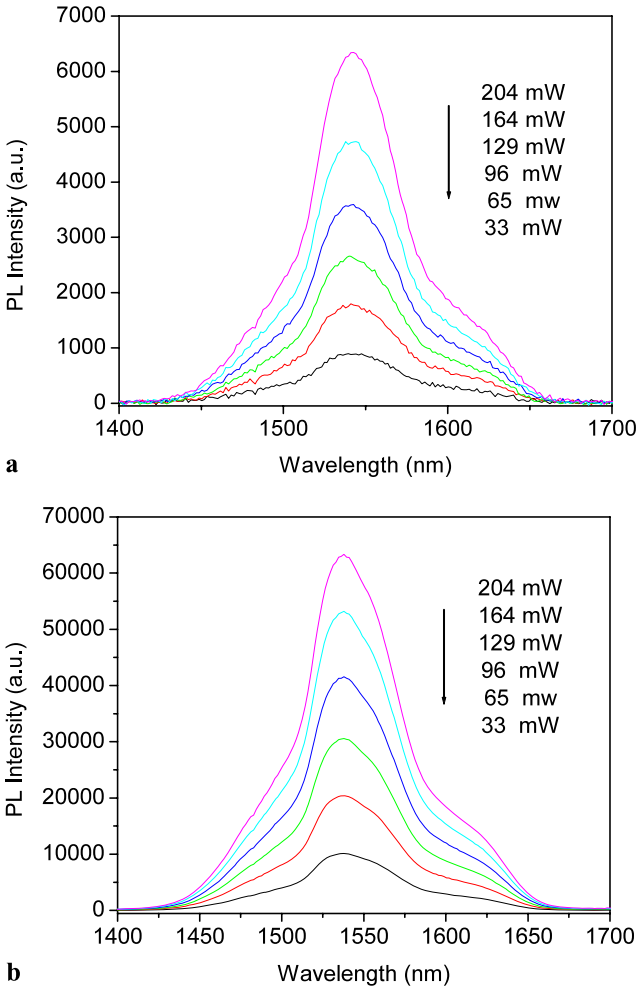

Fig. 3 NIR luminescence of (**a**) $ZnAl_2O_4$:Er and (**b**) $ZnAl_2O_4$:Er, Yb under CW excitation at $\lambda_{exi} = 980$ nm, recorded for different pump excitation power values

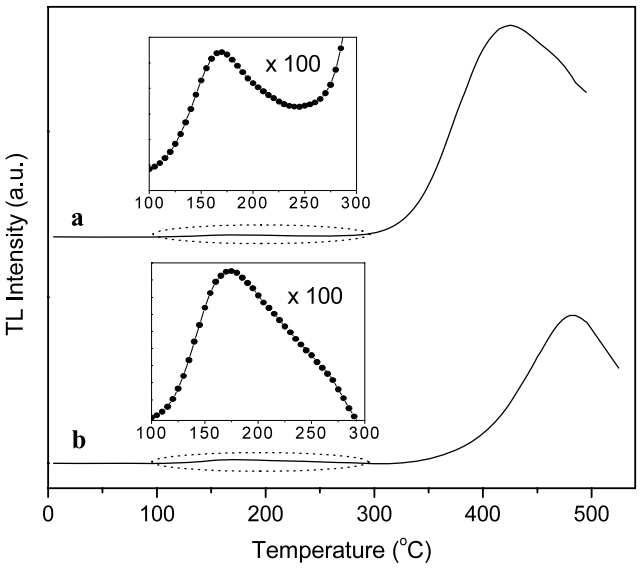

Fig. 4 TSL glow curves of (**a**) $ZnAl_2O_4$:Er and (**b**) $ZnAl_2O_4$:Er, Yb (test gamma dose: 100 Gy); the numbers after X indicate the multiplication factor

a single broad ESR line with an isotropic g-value equal to 2.0003 and 23 gauss linewidth. Not many defect centres are expected to be formed in a system like $ZnAl_2O_4$ and the most probable centres which can be observed are the F^+ centres (an electron trapped at an anion vacancy) and O^- ions (a positive hole localised on O^{2-} ion neighbouring a cation vacancy).

ESR spectrum of the Er^{3+}-doped $ZnAl_2O_4$ exhibits a large linewidth of Centre I indicating an unresolved hyperfine structure. The interaction of the unpaired electron with nearby nuclear spins gives rise to unresolved hyperfine structure. In $ZnAl_2O_4$:Er phosphor, aluminium as well as zinc have isotopes with nuclear spin 5/2: ^{27}Al and ^{67}Zn. ^{27}Al is much more abundant (100%) than ^{67}Zn (4.11%) and its nuclear magnetic moment is higher (3.6385) than that of ^{67}Zn (0.8753) [38]. As aluminium is more abundant, it is very likely that the electronic spin will be interacting with aluminium nuclei. It is known that the cation disorder and non-stoichiometry of aluminates like $ZnAl_2O_4$ provide a large number of lattice defects which may serve as trapping centres. F^+ centres are likely to be formed by trapping of electrons at oxygen vacancies, and hole trapping at aluminium and zinc vacancies could lead to the formation of V centres. The unresolved hyperfine lines which manifest as broad line of Centre I indicate that the unpaired electron is delocalised and interacts with nearby aluminium nuclei. It has been speculated [39] that in oxides, the charges must be trapped near double (or more) charged defects in order for the charge to be delocalised, thus allowing it to interact with surrounding nuclei. Hence Centre I is assigned to an O^- ion stabilised by a nearby cation vacancy (a hole trapped in a Al^{3+}/Zn^{2+} ion vacancy). The unpaired electron in this centre resides mainly in an oxygen $2p_\sigma$ atomic orbital. It may be mentioned that a similar centre in neutron irradiated $MgAl_2O_4$ has also been ascribed to an O^- ion [40].

The stability of Centre I was measured using the pulsed thermal annealing method. After heating the sample up to a given temperature value where it is maintained for 3 minutes, it is cooled rapidly down to room temperature for ESR measurements. The thermal annealing behaviour of Centre I is shown in Fig. 6. It is observed that the centre becomes unstable around 100°C and decays in the temperature range 100°C–250°C. This decay appears to relate to the low temperature TSL peak at 174°C.

The ESR line labelled as II in Fig. 5a is due to a centre characterised by a single ESR line with an isotropic g-value equal to 2.0046 and 7 gauss linewidth. One of the most probable centres which can be trapped in the present system is the F^+ centre. Hutchison [41] first observed such a centre in neutron irradiated LiF. Irradiation leads to the trapping of an electron at an anionic vacancy and such trapping is the basis

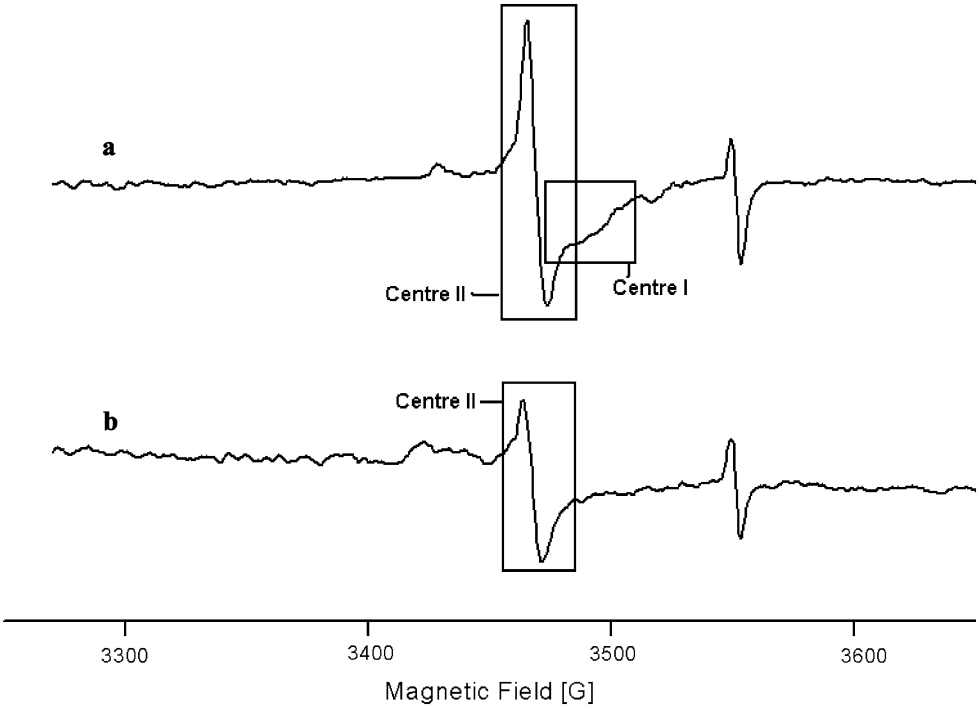

Fig. 5 Room temperature ESR spectra of irradiated (**a**) $ZnAl_2O_4$:Er and (**b**) $ZnAl_2O_4$:Er, Yb phosphors (gamma dose: 5000 Gy). Line labelled as I is due to an O^- ion. The Centre II line is assigned to a F^+ centre

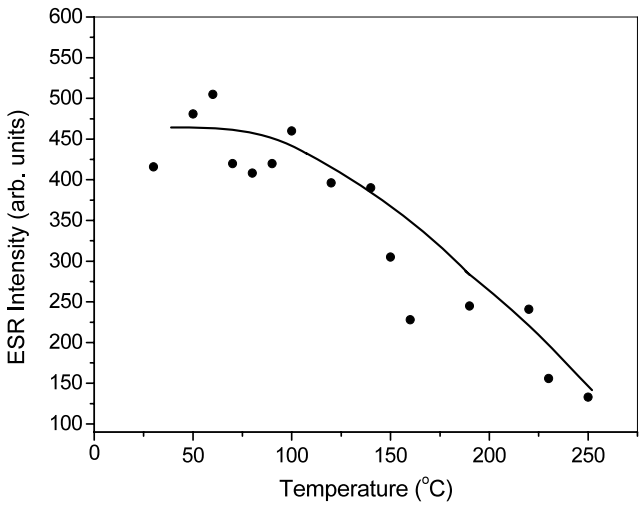

Fig. 6 Thermal annealing behaviour of Centre I in $ZnAl_2O_4$:Er phosphor

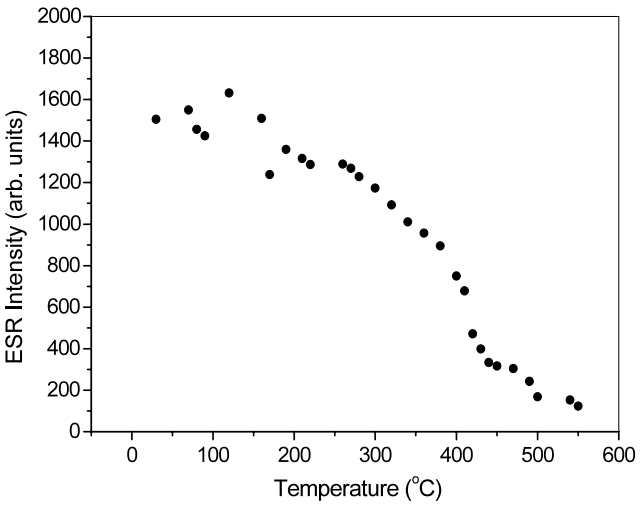

Fig. 7 Thermal annealing behaviour of Centre II in $ZnAl_2O_4$:Er phosphor

for the formation of F^+ centres. Hyperfine interaction with the nearest-neighbour cations is the major contribution to the linewidth. Defect Centre II formed in the present system is characterised by a small g-shift and the linewidth is reasonably large. Unresolved hyperfine structure causes large linewidths. On the basis of these observations and considerations of the characteristic features of the defect centres likely to be formed in a system such as $ZnAl_2O_4$:Er, Centre II is tentatively assigned to a F^+ centre.

The stability of Centre II was measured using the pulsed thermal annealing technique. The thermal annealing behaviour of Centre II is shown in Fig. 7. It is observed that the centre shows two intensity decreasing stages. The first stage is in the temperature range 280°C–430°C and the second stage corresponds to the region 440°C–550°C. The second stage of decay appears to correlate with the high temperature TSL peak at 483°C.

Irradiated Yb co-doped $ZnAl_2O_4$:Er phosphor also exhibits ESR lines due to two defect centres. However, intensity of ESR lines is low and in fact, Centre I ESR line is hardly seen. The observed ESR spectrum is shown in Fig. 5b. Experiments could not be carried out on Centre I

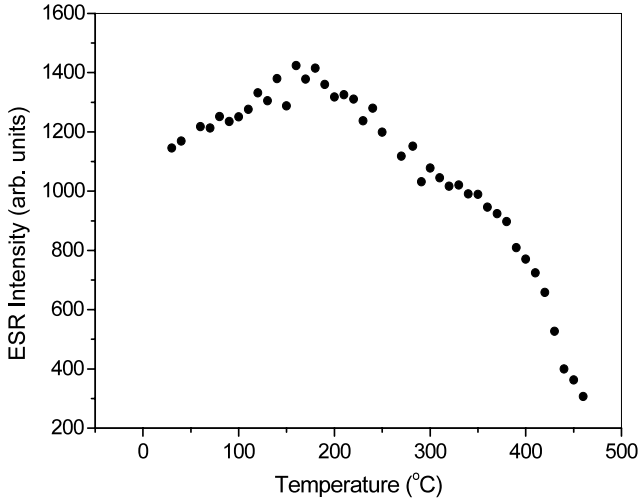

Fig. 8 Thermal annealing behaviour of Centre II in $ZnAl_2O_4$:Er, Yb phosphor

due to its low intensity. Centre II is characterised by a single ESR line with an isotropic g-value equal to 2.0054 and 8 gauss linewidth. The two defect centres are assigned to an O^- ion and F^+ centre on the basis of the reasons mentioned above. The thermal annealing behaviour of Centre II is shown in Fig. 8. It is observed that there are some small intensity changes in the temperature region 100°C to 250°C. However, the actual decay of the centre is seen to take place in the region 360°C to 460°C. This decay appears to correlate with the high temperature TSL peak observed in this phosphor at 423°C. Yb co-doping is found to shift the TSL peaks to low temperatures. It is gratifying to note that the correlated F^+ centre decays at lower temperatures as compared to its behaviour in the $ZnAl_2O_4$:Er phosphor. This is expected if the defect centre indeed correlates with the high temperature TSL peak.

4 Conclusions

The solution combustion method has been successfully implemented for the synthesis of $ZnAl_2O_4$:Er co-doped with Yb^{3+} powders. The synthesis process is instantaneous, which saves energy and time, and a calcination step can be avoided. The EDX analysis shows the peaks due to Zn, Al, O, Er and Yb, which confirmed that the Er and Yb elements were successfully doped into $ZnAl_2O_4$ host. The photoluminescence from Er^{3+} around 1.5 μm is enhanced in $ZnAl_2O_4$ phosphor co-doped with Yb^{3+} upon 980 nm pumping and this may find applications in optical communications. Two defect centres are identified in irradiated $ZnAl_2O_4$:Er and $ZnAl_2O_4$:Er, Yb phosphors with the help of ESR study. These centres are tentatively assigned to an O^- ion and F^+ centre. The O^- ion appears to correlate with the 174°C TSL peak while the F^+ centre appears to relate with the high temperature TSL peak at 483°C in $ZnAl_2O_4$:Er phosphor.

Acknowledgements Vijay Singh gratefully acknowledges the LPQM, ENS de Cachan, (France) for the one-year postdoctoral fellowship. Vijay Singh also gratefully acknowledges Research Assistant Professorship at Chung-Ang University, Seoul (South Korea) from BK21 program. This work has been supported by a grant from the Seoul R&D program (2006). T.K. Gundu Rao is grateful to FAPESP, Brazil for the research fellowship.

References

1. S.K. Sampath, J.F. Cordaro, J. Am. Ceram. Soc. **81**, 649 (1998)
2. W. Strek, P. Deren, E. Lukowiak, B. Nissen, J. Wrzyszcz, M. Zawadzki, P. Pershukevich, Spectrochim. Acta A **54**, 2121 (1998)
3. I. Futoshi, G. Naoyuki, M. Masashi, US Patent 5,561,089 (1996)
4. H. Grabowska, W. Mista, J. Trawczynski, J. Wrzyszcz, M. Zawadzki, Appl. Catal. A, Gen. **200**, 1561 (2001)
5. R. Roesky, J. Weiguny, H. Bestgen, U. Dingerdissen, Appl. Catal. A, Gen. **1976**, 213 (1999)
6. J.F. Cordoro, US Patent 6,099,637 (8 August 2000)
7. S. Mathur, M. Veith, M. Haas, Haoshen, N. Lecerj, V. Huch, J. Am. Ceram. Soc. **84**, 1921 (2001)
8. R.M. Kadam, T.K. Seshagiri, V. Natarajan, S.V. Godbole, Nucl. Instrum. Methods Phys. Res., Sect. B **266**, 5137 (2008)
9. M.A. Reshchikov, H. Morkoç, B. Nemeth, J. Nause, J. Xie, B. Hertog, A. Osinsky, Physica B **401–402**, 358 (2007)
10. Y. Kawabe, A. Yamanaka, H. Horiuchi, H. Takashima, E. Hanamura, J. Lumin. **121**, 517 (2006)
11. K. Tanaka, T. Hosoya, R. Fukaya, J. Takeda, J. Lumin. **122–123**, 421 (2007)
12. V.B. Mikhailik, H. Kraus, D. Wahl, H. Ehrenberg, M.S. Mykhaylyk, Nucl. Instrum. Methods Phys. Res., Sect. A **562**, 513 (2006)
13. I.N. Ogorodnikov, V.A. Pustovarov, M. Kirm, V.S. Cheremnykh, J. Lumin. **115**, 69 (2005)
14. N.D. Nedeoglo, A.N. Avdonin, G.N. Ivanova, D.D. Nedeoglo, G.V. Kolibaba, V.P. Sirkeli, J. Lumin. **112**, 62 (2005)
15. T.K. Gundurao, S.V. Moharil, Radiat. Meas. **42**, 35 (2007)
16. G.M. Hassan, M. Ikeya, S. Takaki, Radiat. Meas. **30**, 189 (1999)
17. D.A.E. Ehlermann, Appl. Radiat. Isot. **47**, 1547 (1996)
18. C.L.P. Mauricio, E. Bortolin, S. Onori, Radiat. Meas. **26**, 639 (1996)
19. S. Soumana, J. Faïn, D. Miallier, M. Montret, Th. Pilleyre, S. Sanzelle, M. Akselrod, Radiat. Meas. **23**, 501 (1994)
20. E. Bortolin, P. Fattibene, C. Furetta, S. Onori, Appl. Radiat. Isot. **44**, 327 (1993)
21. S. Agnello, R. Boscaino, M. Cannas, F.M. Gelardi, J. Non-Cryst. Solids **232–234**, 323 (1998)
22. R.M. Kadam, T.K. Seshagiri, V. Natarajan, S.V. Godbole, Nucl. Instrum. Methods Phys. Res., Sect. B **266**, 5137 (2008)
23. S. Murali, V. Natarajan, T.K. Seshagiri, R.M. Kadam, R. Venkataramani, M.D. Sastry, Radiat. Meas. **37**, 259 (2003)
24. V. Singh, T.K. Gundu Rao, J. Solid State Chem. **181**, 1387 (2008)
25. V. Singh, T.K. Gundu Rao, J.-J. Zhu, J. Lumin. **126**, 1 (2007)
26. V. Singh, T.K. Gundu Rao, J.-J. Zhu, M. Tiwari, Mater. Sci. Eng., B **131**, 195 (2006)
27. K.i. Cho, K.H. Cho, S.H. Cho, D.W. Shin, Opt. Mater. **28**, 888 (2006)
28. G.C. Righini, S. Pelli, M. Brenci, M. Ferrari, C. Duverger, M. Montagna, R. Dall'Igna, J. Non-Cryst. Solids **284**, 223 (2001)
29. J.H. Lee, K. Katoh, K. Kikuchi, Opt. Commun. **266**, 681 (2006)
30. S. Hinojosa, O. Barbosa-García, M.A. Meneses-Nava, J.L. Maldonado, E. de la Rosa-Cruz, G. Ramos-Ortiz, Opt. Mater. **27**, 1839 (2005)

31. J. Zhang, S. Dai, G. Wang, L. Zhang, H. Sun, L. Hu, Phys. Lett. A **345**, 409 (2005)
32. H.-K. Jung, J.-S. Oh, S.-I. Seok, T.-H. Lee, J. Lumin. **114**, 307 (2005)
33. Y.M. Yu, J.J. Ju, M. Cha, J. Cryst. Growth **229**, 175 (2001)
34. Z. Wang, F. Tao, W. Cai, L. Yao, X. Li, Solid State Commun. **144**, 255 (2007)
35. S.R. Jain, K.C. Adiga, V.R. Pai Vernekar, Combust. Flame **40**, 71 (1981)
36. P.G. Kik, A. Polman, Mater. Res. Bull. **23**, 48 (1998)
37. S. Tanabe, N. Sugimoto, S. Ito, T. Hanada, J. Lumin. **87–89**, 670 (2000)
38. R.C. Weast (ed.), *Handbook of Chemistry and Physics* (CRC, Clevlend, 2007)
39. N.Y. Konstantinov, L.V. Karaseva, V.V. Gromov, Dokl. Acad. Nauk. SSR **228**, 631 (1980)
40. V.T. Gritsyna, V.A. Kobyakov, Zh. Tekh. Fiz. **55**, 354 (1985); [Sov. Phys. Tech. Phys. **30**, 206 (1985)]
41. C.A. Hutchison, Phys. Rev. **75**, 1769 (1949)